OPEN ACCESS
Journal of Innovative Optical Health Sciences
Vol. 17, No. 2 (2024) 2350013 (11 pages)

DOI: 10.1142/S179354582350013X

World Scientific
www.worldscientific.com

Microwave-induced thermoacoustic elastic imaging: A simulation study

Lin Huang*,†,‡, Zheng Liang*, Shuaiqi Qiao* and Weipeng Wang*
*School of Electronic Science and Engineering
(National Exemplary School of Microelectronics)
University of Electronic Science and
Technology of China, Chengdu, P. R. China
†Zhangjiang Laboratory
100 Haike Road, Shanghai 201204, P. R. China
‡lhuang@uestc.edu.cn

Received 12 April 2023
Revised 5 May 2023
Accepted 5 May 2023
Published 20 October 2023

Microwave-induced thermoacoustic imaging (MTI) has the advantages of high resolution, high contrast, non-ionization, and non-invasive. Recently, MTI was used in the field of breast cancer screening. In this paper, based on the finite element method (FEM) and COMSOL Multiphysics software, a three-dimensional breast cancer model suitable for exploring the MTI process is proposed to investigate the influence of Young's modulus (YM) of breast cancer tissue on MTI. It is found that the process of electromagnetic heating and initial pressure generation of the entire breast tissue is earlier in time than the thermal expansion process. Besides, compared with normal breast tissue, tumor tissue has a greater temperature rise, displacement, and pressure rise. In particular, YM of the tumor is related to the speed of thermal expansion. In particular, the larger the YM of the tumor is, the higher the heating and contraction frequency is, and the greater the maximum pressure is. Different Young's moduli correspond to different thermoacoustic signal spectra. In MTI, this study can be used to judge different degrees of breast cancer based on elastic imaging. In addition, this study is helpful in exploring the possibility of microwave-induced thermoacoustic elastic imaging (MTAE).

Keywords: Thermoacoustic imaging; breast cancer; multi-physics simulation; elastic imaging.

1. Introduction

Since the 20th century, breast cancer has been one of the most common tumors in the world.[1] In the early stage of breast cancer, through a variety of detection or imaging techniques,[2] it can be effectively detected and controlled by medical methods to improve the survival possibility of patients.[3] Currently, the commonly used medical methods for

breast cancer detection include traditional palpation,[4] mammography,[5] ultrasound (US) imaging,[6] magnetic resonance imaging (MRI),[7] computed tomography (CT),[8] and photoacoustic imaging (PAI).[9] These imaging techniques have their own advantages and shortcomings in breast cancer imaging,[10–15] such as insufficient resolution, low contrast, poor real-time performance, poor imaging specificity, and high detection costs and risks. These disadvantages probably lead to false positives and false negatives in medical diagnosis. Microwave-induced thermoacoustic imaging (MTI) based on the thermoacoustic (TA) effect is considered to be an imaging method with good application prospects in the field of breast cancer detection.[16,17] It combines the characteristics of the high contrast of microwave imaging and the high spatial resolution of US imaging. It also exhibits the merits of non-invasiveness and non-ionization.[18,19]

During the MTI process, the factors affecting TA signals are mainly divided into microwave parameters and biological tissue parameters.[20] In addition to a large number of experimental studies, there are also many theoretical simulation studies in recent years.[21–23] Vasilis Ntziachristos *et al.* used COMSOL software to conduct a simulation study and experimentally validated a near-field radio frequency tomography (NRT) method for high-resolution imaging of biological tissue using ultra-short electromagnetic (EM) pulses.[24] Tony George *et al.* used MTI to investigate early breast cancer detection and used COMSOL to conduct a two-dimensional simulation of MTI signal generation to evaluate the changes in biological tissue temperature and pressure under EM field irradiation.[25] The minimum power required to generate a 2.45 GHz microwave source TA signal at different power levels was evaluated. Mohand Alzuhiri *et al.* proposed a two-dimensional numerical model to simulate the generation of near-field MTI signals.[26] The model simulates the EM interaction of microwaves with imaging targets, as well as the generation and propagation of acoustic signals. The effects of the target's electrical properties, microwave frequency, and pulse duration on the intensity and frequency of the generated acoustic signal were studied. Soltani *et al.* conducted some three-dimensional numerical simulations of the TA imaging phenomenon as a multi-physics problem through COMSOL simulation software.[27] They calculated the corresponding pressure gradients produced by temperature changes generated by EM wave irradiation. In 2020, they continued the numerical study of MTI using COMSOL software for the preliminary detection of Anatomically Realistic Breast Phantom (ARBP) and proposed that the size and shape of the tumor do not significantly affect the TA detection efficiency.[28] However, there is a lack of quantitative research on MTI physical dynamics in breast cancer imaging, especially for the physical parameters of the thermal expansion process.

Based on the finite element method (FEM) and COMSOL Multiphysics software, this paper proposes a three-dimensional breast cancer model which combines the advantages of the ARBP model and is suitable for exploring the MTI process. It explores the physical parameter changes of tumor tissues during MTI. Based on elastic imaging and the state equation of thermoacoustic imaging to determine the theoretical basis of the whole simulation, our work observed the distribution of physical quantities through the physical field simulation of the thermoacoustic process of breast cancer. We then explored the thermoacoustic signals of breast cancer in different periods by changing Young's modulus (YM) of breast cancer through the control variable method. By comparing these signals in the time domain and frequency domain, this paper quantitatively researches the influence of YM on the TA signals. The hardness of breast cancer varies in different periods, which is reflected in the value of YM. Studying the amplitude and frequency of TA signals is beneficial for obtaining high-contrast thermoacoustic images. In the long run, we hope that our work can help diagnose some clinical diseases, such as the size of breast lumps, the different stages of cirrhosis in liver disease, and the classification of plaque in vascular disease.

2. Materials and Methods

2.1. *TA processes and governing equations*

The MTI of biological tissue includes microwave radiation, thermal expansion, and the generation of acoustic waves.[28] First, when a biological tissue is irradiated with pulsed microwave, the tissue will absorb EM energy. To quantify the amount of energy absorbed by different regions of the tissue, the specific absorption rate (SAR) is used to calculate the spatial distribution of the absorbed energy.[29]

The calculation formula of SAR is

$$\mathrm{SAR}(r,t) = \frac{\sigma(r)|\mathbf{E}(r)|^2}{2\rho(r)} e(t). \tag{1}$$

In Eq. (1), $\sigma(S/m)$ represents the electrical conductivity of biological tissues and the electrical conductivity of different biological tissues is different. For example, the difference between tumors and normal breast tissues is large. It leads to differences in absorption of EM energy. In addition, its distribution in biological tissues is also directional. $\mathbf{E}(V/m)$ represents the electric field distribution in the tissue, ρ (kg/m^3) represents the density, and e represents the envelope function of the microwave pulse excitation, $t(s)$ and $r(m)$ represent the time and spatial location of the tissue, respectively.

The EM energy absorbed by the tissue will rapidly heat the tissue, and the temperature change[30] $\Delta T(K)$ is generally described by

$$\Delta T = \frac{\sigma(r)|\mathbf{E}(r)|^2}{2\rho(r)C_p} \tau. \tag{2}$$

In Eq. (2), C_p (J/(kg $\cdot$ K) represents the specific heat capacity at constant volume. $\tau(s)$ represents the pulse width of the EM wave. In the process of MTI, it needs to satisfy two time constraints: thermal conduction constraints and elastic deformation constraints.[31] In practical applications, its value is usually 70–1000 ns due to technical limitations of microwave sources.[32]

The temperature rising inside the tissue will cause thermal expansion of the tissue, and the thermal energy will be converted into elastic potential energy and mechanical energy, resulting in a change in the initial sound pressure distribution.[28,33] This process can be described by governing Eq. (3). Changes in sound pressure inside tissue induce sound waves, known as TA signals. It propagates in all directions within the organization, and this propagation process is described in Eq. (4).

$$\left(1 + \frac{2\alpha_a(r,\omega)c(r)}{\omega^2}\frac{\partial}{\partial t}\right)\nabla \cdot \mathbf{u}(r,t) = \beta(r)\frac{\partial}{\partial t}T(r,t) - \frac{1}{\rho(r)c^2(r)}\frac{\partial}{\partial t}p(r,t), \tag{3}$$

$$\nabla p(r,t) = -\rho(r)\frac{\partial}{\partial t}\mathbf{u}(r,t). \tag{4}$$

In Eqs. (3) and (4), the main factors affecting the generation and propagation of TA signals are the following: α_a (1/m) represents the acoustic attenuation coefficient, which is related to the sound frequency and propagation medium. c (m/s) represents the speed of sound. ω (Hz) represents the angular acoustic frequency. $\boldsymbol{u}$ (m/s) represents the sound velocity vector. β (1/K) stands for the volume thermal expansion coefficient, which is three times the value of the length thermal expansion coefficient. T (K) and p (Pa) stand for temperature and sound pressure, respectively.

2.2. *Theories of breast cancer elastography*

When the breast is diseased, it is often accompanied by changes in mechanical properties[34,35] and the difference in elastic modulus between normal human tissues and diseased tissues can often reach dozens of times, such as breast cancer, prostate cancer, liver cirrhosis, and kidney diseases. In 1991, Ophir first proposed a static stress elastography method and revealed the feasibility of elastography by measuring the distribution of strain and elastic modulus of biological tissues during the experiment.[35] In recent years, for breast cancer imaging, the main elastography techniques are ultrasonic strain elastography (USE),[36] ultrasonic shear wave elastography (USWE),[37] magnetic resonance elastography (MRE),[38] and photoacoustic elastography (PAE).[39]

USE and USWE are the most widely utilized methods clinically. The USE uses external pressure or acoustic radiation force to excite tissue to generate different strain response signals.[35,40] According to the difference in elastic modulus of different tissues, such strains include displacement, acoustic wave velocity, etc. Under the same external force, the degree of strain (such as displacement) caused by the hard tissue with a large elastic modulus is smaller, and the degree of strain caused by the soft tissue with a small elastic modulus is larger. By detecting and collecting tissue responses, the differences in mechanical properties between different tissues can be inverted using appropriate image reconstruction algorithms.

Traditional MTI technology mainly uses the electrical conductivity distribution of different tissues to reconstruct TA images,[41] and applies external EM waves to excite tissue, and further cause thermal expansion inside the tissue to generate a strain. This strain will convert thermal energy into

elastic potential energy and then generate mechanical vibration.[42] The transformation of elastic potential energy can be reflected by quantitative observation of deformation and pressure changes, which is specific to the lesions that cause elastic coefficient changes. This paper also explores the possibility of TA elastography by quantitatively analyzing the effect of tumor YM on the simulation results of MTI.

2.3. *COMSOL strategy*

In this study, the simulation of the MTI process of breast cancer is based on a FEM software COMSOL Multi-physics (version 6.0). The breast cancer model and corresponding parameters of each biological tissue are based on a real 3D breast numerical model library provided by the University of Wisconsin Cross-Disciplinary Electromagnetics Laboratory (UWCEM).[43] The reference model is the ACR Class 2 scattered fibroglandular and its Breast ID is 012204. To simulate the real situation in the process of breast cancer by MTI, and save simulation, the breast cancer model was restored and simplified as much as possible. Figure 1 shows the 3D model used in this study.

In Fig. 1, the size of the tank is 160 mm× 200 mm × 200 mm, and the entire model is placed in the tank filled with transformer oil, which is used as the coupling medium in MTI. The waveguide is a standard BJ32 waveguide.[44] The waveguide is positioned against the tank wall and faces the breast cancer model. The entire appearance of the breast model is simplified into a cube with a size of 100 mm × 100 mm × 100 mm, and the model

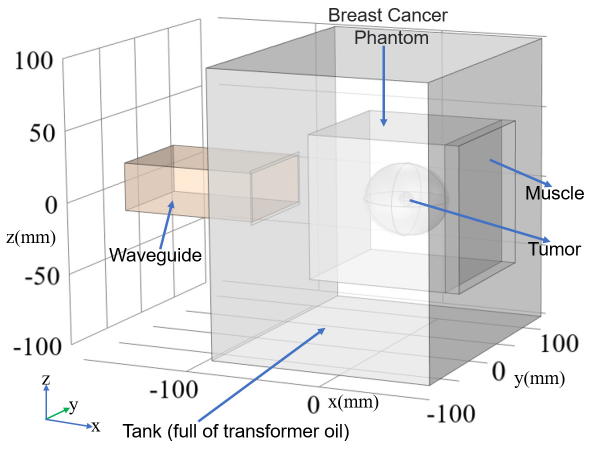

Fig. 1. Simulation model diagram of MTI of 3D breast cancer.

Table 1. Dielectric characteristic parameters of different materials.

Material types	Relative permittivity	Electrical conductivity (S/m)
Transformer oil	5	1.0×10^{-11}
Fat	7	0.5
MG	47	2.2
Muscle	52.73	1.74
Tumor	55	4

includes a fat layer, breast, tumor, and a rightmost pectoral muscle layer from outside to inside. The following breast cancer models specifically refer to the whole composed area of four modules, not individual tumor areas. The size of the mammary gland (MG) is 30 mm × 25 mm × 25 mm. In Fig. 1, the breast muscle is closely connected to the rightmost side of the breast cancer model and the boundary of the fat layer, with a size of 10 mm × 100 mm × 100 mm.

The TA signal is related to the dielectric and thermodynamic properties of different tissues. The materials used in the simulation study,[27,28,33,45–54] including the dielectric properties of transformer oil, are shown in Table 1. The thermodynamic properties of different biological tissues are shown in Table 2, where ρ represents density, C_p represents specific heat capacity, YM (Pa) is the YM, PR is Poisson's ratio, k (W/m · K) is the thermal conductivity, and α (1/K) is the thermal expansion coefficient. These parameters jointly affect the thermal expansion process of breast tissue.

According to the MTI process, three physical field modules are mainly involved in the simulation, namely electromagnetic waves (frequency domain), solid heat transfer, and solid mechanics.[55–59] For the research in the frequency domain, a solver based on a 3.0 GHz carrier is used, and for the research in the transient (time domain), a solver with a simulation time of 0–1 ms with a step size of 1 μs is used.

The boundary conditions in this study include electromagnetic field boundary conditions,[60] heat transfer boundary conditions,[61] and solid mechanics boundary conditions.[62] For the waveguide, its domain-defining material is air, and it inputs EM waves at 3.0 GHz. In the heat-transfer boundary condition, the bottom surface of the muscle layer in the model is determined to be "thermal isolation". In the MTI experiments, the acquisition time is generally longer than the μs-level. The other outer

Table 2. Thermodynamic parameters of different materials.

Tissue types	ρ (kg/m^3)	C_p (J/(kg · K))	α (1/K)	k (W/(m · K))	YM (Pa)	PR
Fat	930	2770	3.0×10^{-5}	0.21	1.8×10^4	0.49
MG	1050	3770	4.5×10^{-5}	0.48	5.0×10^4	0.49
Muscle	1100	3800	4.14×10^{-5}	0.48	4.80×10^5	0.49
Tumor	1050	3852	6.5×10^{-5}	0.54	1.06×10^5	0.49

surfaces of the breast cancer model connected with transformer oil were determined as "convective heat flux" and the value of the heat transfer coefficient was $5\,\mathrm{W/(m \wedge 2 \cdot K)}$. It is consistent with the heat transfer between the breast cancer tissue and transformer oil after heating.[27,60] To define solid mechanics boundary conditions, fat, MG, tumor, and muscle are all considered as linear elastic materials. When the microwave pulse width satisfies the elastic deformation constraint, the ground of the muscle layer is indeed a "fixed constraint". The other outer surfaces of the breast and transformer oil in contact are considered "free".

This study aimed to quantitatively study the effects of tumor YM on the pressure changes of the breast cancer model during the MTI process. In addition, this study selected a baseline model (BM) for the comparison of parametric studies. Its simulation settings are as follows: The microwave pulse excitation is a rectangular pulse with a peak power of 75 kW, and the repetition frequency is 1 kHz, which means the pulse excitation period is 1 ms. The pulse width is 1 μs, and the rising and falling edges are 0.1 μs, respectively. Thus, the total microwave energy is 67.5 mJ. The tumor radius is 1 mm, YM is 1.06×10^5 Pa, and the simulation time is 0–1 ms with a 1 μs step size of the solver.

In elastography, the YM of biological tissue is a critical factor. Under the same external conditions, a larger YM corresponds to a smaller deformation, and a smaller YM corresponds to a larger deformation. For breast cancer detection, the YM of cancerous tissue is generally tens to hundreds of times larger than that of normal glandular tissue. In order to explore the possibility of microwave-induced thermoacoustic elastic imaging (MTAE), the YM of various tumors was set appropriately in this study to observe the displacement, pressure, and corresponding vibration frequency at the tumor center. In the BM, the YM of the tumor is two times that of MG. For a more comprehensive and intuitive analysis, the YM of the tumor was set to be 2 times (BM), 4 times (Y1), 10 times (Y2), 20 times (Y3), 40 times (Y4), and 100 times (Y5) of the MG, respectively.

3. Results

For the transient simulation of the BM model, Fig. 2 shows the distribution of spatial displacement inside the breast cancer at 1 ms. For the pressure change during thermal expansion, Fig. 3 shows the distribution of the pressure change inside the breast cancer at 1 ms.

In order to quantitatively investigate the relationship between the YM of the tumor and MTI, tumor models with various YM values were set up (BM, Y1, Y2, Y3, Y4, and Y5). For these models, the selected domain observation point is the tumor center, the specific simulation data sets are shown in Table 3. Then, Fig. 4 displays the pressure spectrum at the tumor center of each model with different Young's moduli.

The details of the above-mentioned four parameters are defined as follows. Within the simulation time 0–1 ms, when the simulation model starts to be excited by microwave ($t = 0.25$ ms), $\Delta D_{\max}$ is the first maximum displacement offset, $\Delta P_{\max}$ is the first peak value of pressure rise, and f_c represents the response frequency in the pressure spectrogram, which includes two center frequencies f_{c1} and f_{c2}.

4. Discussion

Combined with MTI and elastography theory, this part tries to further analyze the above-mentioned simulation results. First, the results obtained by simulating the MTI process based on the BM are analyzed. Then, the simulation results of different microwave characteristics and tumor characteristics are analyzed. Finally, the relationship between YM of the tumor and MTI is discussed.

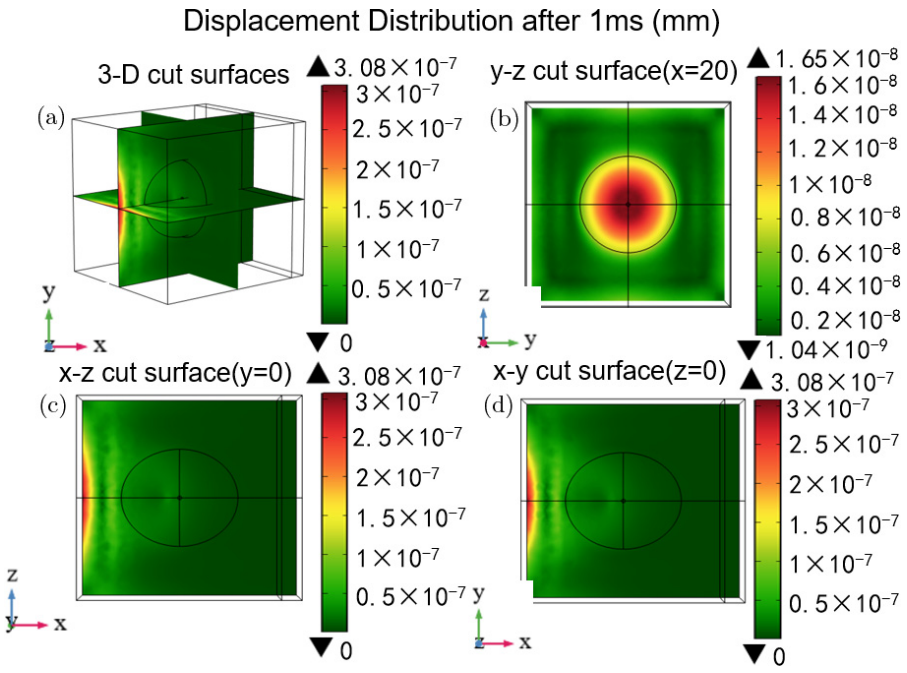

Fig. 2. At $t = 1$ ms, internal displacement distribution of breast cancer area. (a) 3D section, (b) y–z section, (c) x–z section, and (d) x–y section.

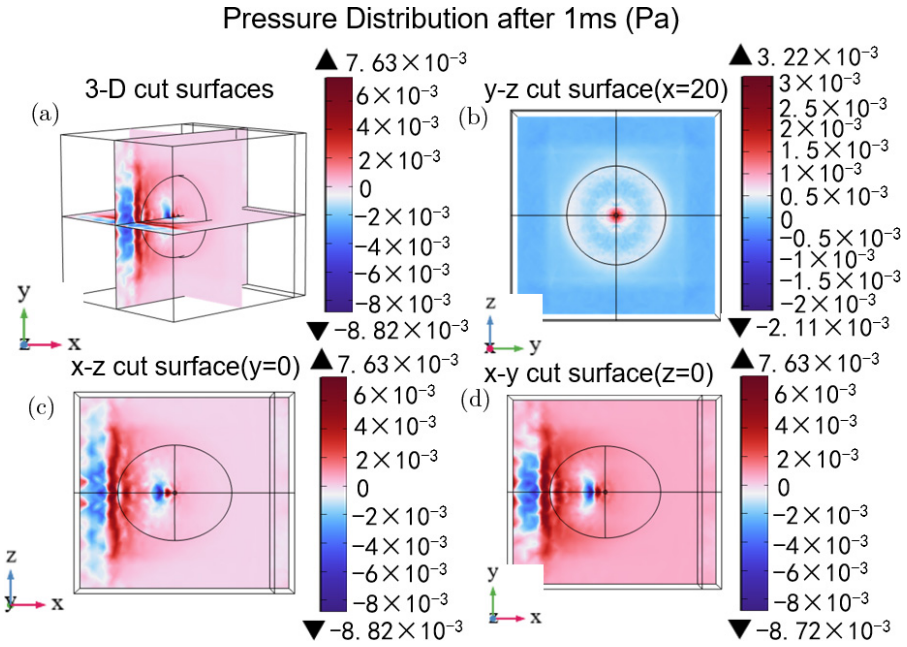

Fig. 3. At $t = 1$ ms, the internal pressure field distribution of the breast cancer area. (a) 3D section, (b) y–z section, (c) x–z section, and (d) x–y section.

4.1. *Analysis of BM results*

The dielectric properties of each tissue in the breast cancer model are different; according to the SAR theory in MTI, the amount of EM energy absorbed by tissue is proportional to its electrical conductivity. Referring to Table 2, the electrical conductivity of a tumor is 4 S/m, which is greater than that of other tissues, so the tumor will absorb more EM energy.

According to the electromagnetic heat theory, the temperature of the tumor is higher than that of

Table 3. Result datasets for tumors with different Young's moduli.

YM ratio	ΔD_{max}(mm) Timing (ms)	ΔP_{max}(Pa) Timing (ms)	f_{c1} (kHz) f_{c2} (kHz)
BM	1.615×10^{-8}	0.0099	24
	1	0.264	43.882
Y1	1.6004×10^{-8}	0.0225	33.288
	1	0.26	59.920
Y2	1.6111×10^{-8}	0.0618	46.604
	1	0.257	94.540
Y3	1.6015×10^{-8}	0.1243	65.246
	1	0.255	130.492
Y4	1.6039×10^{-8}	0.2035	91.877
	1	0.254	181.091
Y5	1.5992×10^{-8}	0.3867	141.145
	1	0.252	284.953

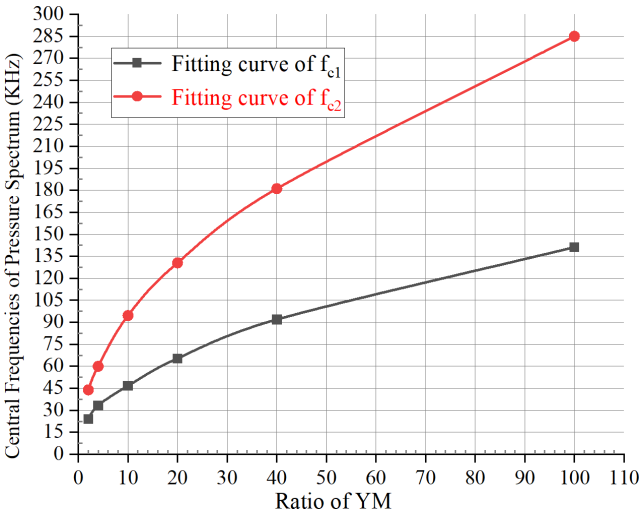

Fig. 4. Pressure spectrum of observation point A of tumors with different Young's moduli.

the surrounding breast tissue, which means that the tumor expands more thermally. According to the theory of elastography, the larger the YM, the smaller the deformation will achieve under the same external force. However, the coefficient of thermal expansion represents the ability of the tissue to expand when heated, and the larger the coefficient of thermal expansion, the greater the length of the tissue increases for the same temperature increase. According to Table 2, $\eta = \alpha/\text{YM}$ is defined to indicate the ability of the tissue to be deformed by heat, then the η values of fat, MG, and tumor are 1.67×10^{-9}, 0.9×10^{-9}, and 0.6×10^{-9}, respectively. Therefore, fat has the strongest thermal deformation ability. As shown in Fig. 2, at 1 ms, the displacement near the tumor is all larger because the temperature rise near the tumor is greater than that of the breast.

Different temperature increases of tissues will lead to different degrees of thermal expansion, which will induce different pressures of tissues. As can be seen from Fig. 3, at 1 ms, the pressure rising in the entire breast cancer and tumor center model has a maximum value of 7.63×10^{-3} Pa and 3.22×10^{-3} Pa, respectively. In addition, at 1 ms, the main areas of pressure increase were the junction area of fat, MG, and the left half of the tumor, while the main areas of pressure decrease were the fat and the left edge of the tumor. At different times, the temperature, displacement, and pressure of different tissues will change. During the MTI process, the change of pressure difference of different tissues will lead to the formation of pressure waves. Pressure waves, or acoustic waves, are mechanical waves that spread in all directions in tissues. They can be collected by ultrasonic transducers in MTI experiments.

Through quantitative analysis, it can be verified that the conductivity of breast cancer tissue deeply affects the absorption of microwave energy, which is consistent with the SAR theory. Different tissues are affected by the elastic modulus and there are differences in the distribution of displacement and pressure in the process of thermal expansion. Moreover, the time points at which each parameter in Table 3 appears further reflect the mechanism, which means that the occurrence time of local displacement and local pressure is different in the time domain and the displacement lags behind the pressure. For the traditional MTI experimental system, more attention is paid to the sound wave after displacement. The change of pressure in the TA process is easy to be ignored. Through this simulation, the acquisition devices of the MTI experiment can be optimized to obtain better TA images.

4.2. *Effect of tumor YM*

According to Table 3, when the YM of the tumor is changed from BM (2 times) to Y5 (100 times), for ΔD_{max}, at 1 ms, the values of each model are consistent. According to the elastic imaging theory, when YM of the tumor increases, the tumor will become more rigid. Moreover, the speed of displacement change will be faster, reflecting the faster thermal expansion, and heat transfer shrinkage of

tumors with larger YM. By analyzing Fig. 4 and Table 3, it can be concluded that when the YM of the tumor increases, the frequency of the tumor pressure change is higher, and the peak pressure $\Delta P_{\max}$ at the tumor is also larger. Figure 4 reflects that the pressure center frequencies f_{c1} and f_{c2} at the tumor center both increase linearly with the increase of YM and the value of proportionality coefficient is about 1.4. In addition, the speed of tissue thermal expansion and contraction is related to the value of YM. More importantly, in the analysis of different models, the relationships between the pressure spectrum of each tissue are tumor > MG > fat, and their YM is also tumor > MG > fat.

The hardness of breast cancer varies greatly in different periods, which will lead to the increase of YM, and the differentiation of gland regions is different. Due to the limitation of imaging resolution and the simplicity of image reconstruction by simply relying on the amplitude of the TA signal, the problem of false positives may occur. Therefore, traditional MTI cannot distinguish different differentiated regions well. Through the research on YM of breast cancer in this paper, the corresponding relationship between TA signal frequency and different Young's Moduli can be established, which is helpful for better reconstruction of TA images, which can solve some similar problems, such as cirrhosis.

5. Conclusions

Aiming at the main physical processes in the MTI, EM energy absorption and thermal expansion process to generate acoustic waves, this paper established a real three-dimensional simulation model of breast cancer in MTI, combining electromagnetic waves (frequency domain), solid heat transfer, and solid mechanics to study the distribution of multiple physical fields within a breast cancer model. By analyzing the abundant simulated datasets, frequency, and time domain plots, the conclusions that can be drawn are as follows: The displacement and pressure of tissue thermal expansion are related to YM and thermal expansion coefficient. The smaller the YM, the greater the thermal expansion coefficient, the greater the displacement of the tissue, and the smaller the pressure rise. The larger the YM, the greater the frequency of thermal expansion and contraction and the greater the maximum pressure. Different stages of tumor development correspond to different Young's moduli, and the TA signal amplitudes and spectrograms obtained by MTI are different, which is beneficial to breast cancer imaging and staging. This paper helps to provide theoretical and numerical guidance for MTI of breast cancer detection and helps to explore the possibility of MTAE via YM calculation, which can further improve the sensitivity and specificity of breast cancer detection, cirrhosis, and vascular plaque diseases.

Acknowledgments

This study was supported in part by the National Natural Science Foundation of China (82071940) and Medico-Engineering Cooperation Funds from the University of Electronic Science and Technology of China (ZYGX2021YGLH205).

Conflicts of Interest

The authors have no conflicts to disclose.

References

1. R. L. Siegel, K. D. Miller, N. S. Wagle, A. Jemal, "Cancer statistics," *Cancer J. Clin.* **71**, 17–48 (2023).
2. A. Jemal, F. Bray, M. M. Center, J. Ferlay, E. Ward, D. Forman, "Global cancer statistics," *CA Cancer J. Clin.* **61**, 69 (2011).
3. A. G. Waks, E. P. Winer, "Breast cancer treatment: A review," *JAMA* **321**, 288 (2019).
4. L. Mahoney, A. Csima, "Efficiency of palpation in clinical detection of breast cancer," *CAMJ* **127**, 729 (1982).
5. J. C. BailarIII, "Mammography: A contrary view," *Ann. Intern. Med.* **84**, 77–84 (1976).
6. R. Guo, G. Lu, B. Qin, B. Fei, "Ultrasound imaging technologies for breast cancer detection and management: a review," *Ultrasound Med. Biol.* **44**, 37–70 (2018).
7. S. C. Rankin, "MRI of the breast," *Brit. J. Radiol.* **73**, 806–818 (2000).
8. B. Zangheri, C. Messa, M. Picchio, L. Gianolli, C. Landoni, F. Fazio, "PET/CT and breast cancer," *Eur. J. Nucl. Med. Mol. Imag.* **31**, 135–142 (2004).
9. R. A. Kruger, C. M. Kuzmiak, R. B. Lam, D. R. Reinecke, S. P. Del Rio, D. Steed, "Dedicated 3D

photoacoustic breast imaging," *Med. Phys.* **40**, 113301 (2013).
10. E. Warner, D. B. Plewes, R. S. Shumak, G. C. Catzavelos, L. S. Di Prospero, M. J. Yaffe, "Comparison of breast magnetic resonance imaging, mammography, and ultrasound for surveillance of women at high risk for hereditary breast cancer," *J. Clin Oncol.* **19**, 3524–3531 (2001).
11. E. Warner, D. B. Plewes, K. A. Hill, P. A. Causer, J. T. Zubovit, R. A. Jong, M. R. Cutrara, G. Deboer, M. J. Yaffe, S. J. Messner, "Surveillance of BRCA1 and BRCA2 mutation carriers with magnetic resonance imaging, ultrasound, mammography, and clinical breast examination," *JAMA* **292**, 1317–1325 (2004).
12. M. Säbel, H. Aichinger, "Recent developments in breast imaging," *Phys. Med. Biol.* **41**, 315 (1996).
13. L. Liberman, T. L. Feng, D. D. Dershaw, E. A. Morris, A. F. Abramson, "US-guided core breast biopsy: use and cost-effectiveness," *Radiology* **208**, 717–723 (1998).
14. D. Grosenick, H. Rinneberg, R. Cubeddu, P. Taroni, "Review of optical breast imaging and spectroscopy," *J. Biomed. Opt.* **21**, 091311 (2016).
15. L. Liberman, A. F. Abramson, F. B. Squires, J. R. Glassman, E. A. Morris, D. D. Dershaw, "The breast imaging reporting and data system: positive predictive value of mammographic features and final assessment categories," *AM. J. Roentgenol.* **171**, 35–40 (1998).
16. X. Wang, R. S. Witte, H. Xin, "Thermoacoustic applications in breast cancer imaging, non-contact explosive detection and communications," in *2015 Asia-Pacific Microwave Conf. (APMC)*. pp. 1–2, IEEE (2015).
17. Z. X. Luo, C. Z. Li, D. T. Liu, B. S. Wang, L. J. Zhang, Y. X. Ma, K. W. Xu, X. Wang, "Quantitative reconstruction of dielectric properties based on deep-learning-enabled microwave-induced thermoacoustic tomography," *IEEE Trans. Microw. Theory* **1**, 1–12 (2023).
18. C. Z. Li, Z. J. Xi, G. F. Jin, W. C. Jiang, B. S. Wang, X. R. Cai, X. Wang, "Deep-learning-enabled microwave-induced thermoacoustic tomography based on ResAttU-net for transcranial brain hemorrhage detection," *IEEE Trans. Bio-Med. Eng.* **1**, 1–12 (2023).
19. Y. J. Li, S. X. Zhang, L. H. Wu, Z. W. Cheng, Z. H. Zhang, H. H. Wang, S. X. Zhao, M. Y. Ren, S. H. Yang, D. Xing, H. Qin, "Polarization microwave-induced thermoacoustic imaging for quantitative characterization of deep biological tissue microstructures," *Photon. Res.* **10**, 1297–1306 (2022).
20. L. H. Wu, Z. W. Cheng, Y. Z. Ma, Y. J. Li, M. Y. Ren, D. Xing, H. Qin, "A handheld microwave thermoacoustic imaging system with an impedance matching microwave-sono probe for breast tumor screening," *IEEE Trans. Med. Imaging.* **41**, 1080–1086 (2022).
21. S. X. Zhao, H. H. Wang, Y. J. Li, L. M. Nie, S. X. Zhang, D. Xing, H. Qin, "Ultrashort-pulse-microwave excited whole-breast thermoacoustic imaging with uniform field of large size aperture antenna for tumor screening," *IEEE Trans. Bio-Med. Eng.* **69**, 725–733 (2022).
22. M. Y. Ren, Z. W. Cheng, L. H. Wu, H. M. Zhang, S. X. Zhang, X. Y. Chen, D. Xing, H. Qin, "Portable microwave-acoustic coaxial thermoacoustic probe with miniaturized Vivaldi antennas for breast tumor Screening," *IEEE Trans. Bio-Med. Eng.* **70**, 175–181 (2023).
23. D. Wu, L. Huang, M. S. Jiang, B. H. Jiang, "Contrast agents for photoacoustic and thermoacoustic imaging: a review," *Int. J. Mol. Sci.* **15**, 23616–23639 (2014).
24. D. Razansky, S. Kellnberger, V. Ntziachristos, "Near-field radiofrequency thermoacoustic tomography with impulse excitation," *Med. Phys.* **37**, 4602–4607 (2010).
25. T. George, E. Rufus, Z. C. Alex, "Simulation of microwave induced thermo-acoustical imaging technique for cancer detection," *ARPN J. Eng. Appl. Sci.* **10**, 9424–9428 (2015).
26. M. Alzuhiri, Y. Deng, M. Golkowski, R. Jacobs, "Numerical model for microwave induced thermoacoustic imaging," in *2016 United States National Committee of URSI National Radio Science Meeting (USNC-URSI NRSM)*, pp. 1–2IEEE (2016).
27. M. Soltani, R. Rahpeima, F. M. Kashkooli, "Breast cancer diagnosis with a microwave thermoacoustic imaging technique — a numerical approach," *Med. Biol. Eng. Comput.* **57**, 1497–1513 (2019).
28. R. Rahpeima, M. Soltani, F. M. Kashkooli, "Numerical study of microwave induced thermoacoustic imaging for initial detection of cancer of breast on anatomically realistic breast phantom," *Comput. Meth. Prog. Biomed.* **196**, 105606 (2020).
29. S. A. Winkler, P. A. Picot, M. M. Thornton, B. K. Rutt, "Direct SAR mapping by thermoacoustic imaging: A feasibility study," *Magn. Reson. Med.* **78**, 1599–1606 (2017).
30. International Commission on Non-Ionizing Radiation Protection, "Guidelines for limiting exposure to time-varying electric, magnetic, and electromagnetic fields (up to 300 GHz). International Commission on Non-Ionizing Radiation Protection," *Health Phys.* **74**, 494–522 (1994).
31. L. V. Wang, H. I. Wu, "Ultrasound-modulated optical tomography," *Biomedical Optics: Principles and Imaging*, John Wiley & Sons, New Jersey (2012).
32. S. Liu, Z. Zhao, X. Zhu, Z. L. Wang, Q. H. Liu, "Analysis of short pulse impacting on microwave

induced thermo-acoustic tomography," *Prog. Electromagn. Res.* **61**, 37–46 (2016).
33. X. Wang, "Thermoacoustic applications in breast cancer detection and communications," *Thermoacoustic Applications in Breast Cancer Detection and Communications*, The University of Arizona, Arizona (2014).
34. J. L. Gennisson, T. Deffieux, M. Fink, M. Tanter, "Ultrasound elastography: Principles and techniques," *Diagn. Interv. Imag.* **94**, 487–495 (2013).
35. J. Ophir, S. K. Alam, B. Garra, "Elastography: Ultrasonic estimation and imaging of the elastic properties of tissues," *Proc. Inst. Mech. Eng. H* **213**, 203–233 (1999).
36. W. Khaled, H. Ermert, "Ultrasonic strain imaging and reconstructive elastography for biological tissue," in *Bioengineering in Cell and Tissue Research.* pp. 103–132, Springer (2008).
37. J. Zhou, Y. Lin, J. H. Zhang, X. X. Si'tu, J. Wang, W. Y. Pan, Y. L. Wang, "Reliability of shear wave elastography for the assessment of gastrocnemius fascia elasticity in healthy individual," *Sci. Rep.* **12**, 1–9 (2022).
38. Y. Haas, M. P. Dosch, T. J. Vogl, "Response comparison of PLC and SLC with magnetic resonance elastography after TACE," *Sci. Rep.* **12**, 1–10 (2022).
39. P. Hai, J. Yao, G. Li, C. Li, L. V. Wang, "Photoacoustic elastography," *Opt. Lett.* **41**, 725–728 (2016).
40. R. M. Sigrist, J. Liau, A. El Kaffas, M. C. Chammas, J. K. Willmann, "Ultrasound elastography: Review of techniques and clinical applications," *Theranostics* **7**, 1303 (2017).
41. L. Huang, L. Yao, L. Liu, J. Rong, H. B. Jiang, "Quantitative thermoacoustic tomography: Recovery of conductivity maps of heterogeneous media," *Appl. Phys. Lett.* **101**, 244106 (2012).
42. J. A. Hildebrand, "Thermoacoustic generation in anisotropic media," *J. Acoust. Soc. Am.* **79**, 1457–1460 (1986).
43. M. J. Burfeindt, T. J. Colgan, R. O. Mays, D. S. Jacob, B. Nader, D. B. Van Veen, S. C. Hagness, *IEEE Antennas Wirel. Propag. Lett.* **11**, 1610–1613 (2012).
44. N. Marcuvitz, "Waveguide handbook," *Waveguide Handbook*, Iet (1951).
45. R. W. Pryor, "Multiphysics modeling using COMSOL® v.4 - A first principles approach," *Multiphysics Modeling Using COMSOL®: A First Principles Approach*, Jones & Bartlett Publishers (2009).
46. M. A. Saied, S. H. Mansour, M. Z. El Sabee, A. L. G. Saad, K. N. Abdel-Nour, "Some electrical and physical properties of castor oil adducts dissolved in 1-propanol," *J. Mol. Liq.* **172**, 1–7 (2012).
47. M. Lazebnik, D. Popovic, L. McCartney, C. B. Watkins, J. L. Mary, J. Harter, S. Sewall, A. Magliocco, H. B. John, O. Michal, "A large-scale study of the ultrawideband microwave dielectric properties of normal breast tissue obtained from reduction surgeries," *Phys. Med. Biol.* **52**, 6093 (2007).
48. E. Zastrow, S. C. Hagness, B. D. Van Veen, "3D computational study of non-invasive patient-specific microwave hyperthermia treatment of breast cancer," *Phys. Med. Biol.* **55**, 3611–3629 (2010).
49. Y. Xie, B. Guo, J. Li, G. Ku, L. V. Wang, "A large-scale study of the ultrawideband microwave dielectric properties of normal breast tissue obtained from reduction surgeries," *IEEE Trans. Biomed. Eng.* **55**, 2741–2752 (2008).
50. Y. E. Mohammed, A. G. Saber, "Estimation of E-field inside muscle tissue at MICS and ISM frequencies using analytic and numerical methods," *J. Biomed. Eng. Technol.* **2**, 9–33 (2014).
51. E. Zastrow, S. K. Davis, M. Lazebnik, F. Kelcz, B. D. Van Veen, S. C. Hagness, "Estimation of E-field inside muscle tissue at MICS and ISM frequencies using analytic and numerical methods," *IEEE Trans. Biomed. Eng.* **55**, 2792–2800 (2008).
52. L. Zhou, X. Li, S. Zhu, B. He, "Magnetoacoustic tomography with magnetic induction (MAT-MI) for breast tumor imaging: numerical modeling and simulation," *Phys. Med. Biol.* **56**, 1967 (2011).
53. M. T. Ahmadian, A. A. Nikooyan, "Modeling and prediction of soft tissue directional stiffness using in vitro force displacement data," *Sci. Res.* **16**, 385–389 (2006).
54. A. Chanmugam, R. Hatwar, C. Herman, "Thermal analysis of cancerous breast model," *ASME Int. Mech. Eng. Cong. Expos.* **45189**, 135–143 (2012).
55. K. H. Lim, J. H. Lee, Q. H. Liu, "Thermoacoustic tomography forward modeling with the spectral element method," *Med. Phys.* **35**, 4–12 (2008).
56. H. Hu, T. Zhu, J. Xu, "Model for thermoacoustic emission from solids," *Appl. Phys. Lett.* **96**, 214101 (2010).
57. T. Qin, X. Wang, H. Meng, Y. Qin, B. Webb, G. B. Wan, R. S. Witte, H. Xin, "Experimental validation of a numerical model for thermoacoustic imaging applications," *IEEE Antennas Wirel. Propag. Lett.* **14**, 1235–1238 (2014).
58. F. Gao, Y. Zheng, X. Feng, C. D. Ohl, "Thermoacoustic resonance effect and circuit modelling of biological tissue," *Appl. Phys. Lett.* **102**, 063702 (2013).
59. M. S. Aliroteh, A. Arbabian, "Microwave-induced thermoacoustic imaging of subcutaneous vasculature with near-field RF excitation," *IEEE Trans. Microwave Theory Tech.* **66**, 577–588 (2017).

60. M. W. Kennedy, S. Akhtar, J. A. Bakken, R. E. Aune, "Analytical and experimental validation of electromagnetic simulations using comsol®, re inductance, induction heating and magnetic fields," in: *COMSOL Users Conference*, pp. 1–9, Stuttgart Germany (2011).
61. V. Gerlich, K. Sulovská, M. Zálešák, "COMSOL Multiphysics validation as simulation software for heat transfer calculation in buildings: Building simulation software validation," *Measurement* **46**, 2003–2012 (2013).
62. D. W. Pepper, J. C. Heinrich, "The finite element method: Basic concepts and applications," *The Finite Element Method: Basic Concepts and Applications with MATLAB®, MAPLE, and COMSOL*, CRC Press, Boca Raton (2017).